



Proteasome inhibitor induced SIRT1 deacetylates GLI2 to enhance hedgehog signaling activity and drug resistance in multiple myeloma

Ying Xie¹ · Jing Liu¹ · Hongmei Jiang¹ · Jingya Wang¹ · Xin Li¹ · Jingjing Wang¹ · Shuai Zhu¹ · Jing Guo¹ · Tao Li² · Yuping Zhong³ · Qiguo Zhang⁴ · Zhiqiang Liu¹

Received: 22 July 2019 / Revised: 18 September 2019 / Accepted: 19 September 2019
© The Author(s), under exclusive licence to Springer Nature Limited 2019

Abstract

Multiple myeloma (MM) is still incurable despite the successful application of proteasome inhibitors in clinic. Bortezomib represents the most common chemotherapy for MM, whereas acquired drug resistance and eventually developed relapse remain the major obstruction. In the current study, we established bortezomib-resistant myeloma cell lines and screened gene expression profiles using single cell RNA-sequencing. Resistant MM cells exhibited increased clonogenic potential, specific metabolic, and epigenetic signatures, along with the self-renewal signaling characteristic of MM stem-like cells. Aberrant activation of hedgehog (Hh) signaling was correlated with drug resistance and stem cell-like transcriptional program. The key transcriptional factor GLI2 of the Hh pathway was restricted in the high acetylation and low ubiquitination states in bortezomib-resistant myeloma cells. Further investigation revealed that SIRT1 deacetylates and stabilizes GLI2 protein at lysine 757 and consequentially activates the Hh signaling, and itself serves as a direct target of Hh signaling to format a positive regulating loop. Using combination screening with an epigenetic compound library, we identified the SIRT1 specific inhibitor S1541 and S2804 had very obvious synergetic antimyeloma effect. Sirt1 inhibition could partially impeded the Hh pathway and conferred bortezomib sensitivity in vitro and in vivo. Notably, elevated SIRT1 level was also a prominent hallmark for the resistant myeloma cells, and this expression pattern was confirmed in myeloma patients, but independent of RAS/RAF mutations. Clinically, SIRT1 expression in patients with complete response was suppressed but elevated in relapsed patients, and retrospective analysis showed patients with higher SIRT1 expression had poorer outcomes. In conclusion, the cooperation of SIRT1 and Hh is an important mechanism of drug resistance in myeloma, and therapeutics combining SIRT1 inhibitors will sensitize myeloma cells to proteasome inhibitors.

These authors contributed equally: Ying Xie, Jing Liu

Supplementary information The online version of this article (<https://doi.org/10.1038/s41388-019-1037-6>) contains supplementary material, which is available to authorized users.

✉ Zhiqiang Liu
zhiqiangliu@tmu.edu.cn

- ¹ Department of Physiology and Pathophysiology, School of Basic Medical Science, Tianjin Medical University, Heping, Tianjin 300070, China
- ² School of Medicine, Hunan Normal University, Changsha, Hunan 410006, China
- ³ Department of Hematology, Myeloma Research Center of Beijing, Beijing Chao-Yang Hospital, Capital Medical University, Chaoyang, Beijing 100020, China
- ⁴ Department of Hematology, Nanjing Drum Tower Hospital, Nanjing University, Nanjing, Jiangsu 210008, China

Introduction

Multiple myeloma (MM) is the second most common hematologic malignancy featured by monoclonal proliferation of terminally differentiated plasma cells in the bone marrow and resultant osteolytic bone lesion due to the monoclonal immunoglobulin protein accumulation in most patients [1]. With the development of new reagents, the overall response rates, progression-free survival and overall survival of myeloma patients have been all dramatically improved over the past 15 years [2]. Proteasome inhibitors, such as bortezomib, are the most well studied novel reagents targeting myeloma in clinic. However, in parallel with the development and clinical use of these therapy regimens is the emergence of acquired drug resistance, and eventually the occurrence of resistance to treatment, which makes management of relapsed and refractory myeloma

challenging, and highlights an urgent need to decipher the underlying mechanisms of acquired drug resistance and develop novel strategies that achieve response in refractory patients [3].

Due to the extensive application of the first-in-class proteasome inhibitor in clinic, great details of resistance mechanisms to bortezomib have been investigated. Known mechanisms for acquired drug resistance includes cancer stem cells, aberrant activation of key signaling pathways, enhanced drugs efflux ability, activation of endoplasmic reticulum stress, bone marrow microenvironment, and so on [4]. Of them, abnormal hedgehog (Hh) signaling activation have been emphasized in myeloma and other hematological neoplasms [5], and our previous studied also revealed both canonical and noncanonical activation of Hh signaling contributed to the drug resistance in MM [6, 7]. However, the constitutive mechanisms are still obscure due to the complicated activation ways of Hh signaling, especially the modifications of the key transcriptional factor GLI2.

Among all efforts to overcome drug resistance in patients with relapsed or refractory myeloma, the application of deacetylase inhibitors (DACi) has been highlighted recently for their unique antimyeloma effects through targeting of histone deacetylases (HDACs) [8, 9]. Ample studies have indicated promising perspective of HDACi in management of hematologic cancers, and there have been 17 HDACs in clinical trials concerning the myeloma management [10]. Despite the remarkable antimyeloma effect in preclinical studies, adverse effects of HDAC inhibitors have been reported, which limits the implications of HDAC inhibitors in clinic [11, 12]. Therefore, clarification the roles of HDACs in acquired drug resistance of MM and screening of more specific inhibitors become extra urgent. Of seven members of the class III HDACs (SIRT1-7) [13], SIRT1 is preferentially a nuclear deacetylase, while SIRT2 is primarily a cytosolic deacetylase and SIRT3 is a major regulator of mitochondrial function due to its subcellular localization [14]. SIRT1 modulates both histones and non-histone proteins, such as p53, NF- κ B, FOXO3a, PPAR γ , PGC-1 α , to alter cellular metabolism and responses to stress, and extensive effects of SIRT1 in cell growth, metabolism, apoptosis, autophagy, DNA damage repair, and cell senescence are well delineated [15]. Recently Canettieri et al. reported that mouse Gli family proteins could be acetylated by P300 and deacetylated by HDAC1 [16], and the acetylation modification was correlated with ubiquitination for proteasome degradation [17]. Chauhan et al. reported that inhibition of SIRT1 impaired bortezomib-induced resistance in myeloma cells through increasing the reactive oxygen species, decreasing in vascular endothelial growth factor-induced migration and angiogenesis, as well as abrogation of the NF- κ B signaling

pathway [18]. However, regulation of SIRT1 and the correlation with Hh signaling activation has not been studied.

In the current study, using the established bortezomib-resistant (BR) cell lines and single cell sequencing analysis platform, we intend to explore the expression pattern of HDACs in BR myeloma cells, and investigate the underlying roles in regulation the activation of Hh signaling through posttranscriptional modification of the key transcriptional factor GLI2, and evaluate the efficacy of SIRT1 inhibitor on overcoming bortezomib resistance in myeloma.

Results

Activation of Hh signaling is a key feature of BR MM cells

To investigate the features and mechanisms of PI-induced drug resistance in myeloma cells, we established four BR myeloma cell lines, ANBL-6, H929, MM.1S, and OPM-2, using modified method according to a previous report [19]. After 4 months of induction, we examined the sensitivity to bortezomib, and found of these cell lines the BR MM.1S and BR OPM-2 cells had the highest IC₅₀ fold changes compared with the WT cells (Fig. 1a). We screened 286 highly upregulated and 75 significantly downregulated genes using RNA-sequencing, and the Kyoto Encyclopedia of Genes and Genomes (KEGG) analysis indicated some enriched pathways, such as cell adhesion molecules, the Hh signaling, and hematopoietic cell lineage (Fig. 1b). Consistent with the enrichment results, we found some highly expressed genes, such as *BCL2*, *GLI1*, *SNAI1*, *PTCH1*, *CCND1*, *ABCG2*, and *MYC* were Hh signaling targets, and some were cancer stem cell related, such as *WNT5a*, *ABCB5*, *DLX5*, *HAS1*, and *TCF4* (Fig. 1c) [20]. These gene expressions were also been confirmed by real-time PCR in WT and BR MM.1S and OPM-2 cells (Fig. 1d). To confirm the stemness features of the BR cells, we inoculated WT and BR MM.1S cells into NOD.*Cg-Prkdc^{scid}Il2rg^{tm1Wjl}/SzJ* mice with gradually diluted amount of cells, and found 1×10^7 WT and BR cells initiated almost the same tumor formation rate, but 1×10^6 BR cells generated obvious higher tumor formation rate than the WT cells, and only 1×10^5 BR cells could initiate tumor formation (Fig. 1e). These data suggested BR MM cells have stronger stemness features, since cancer stem cells are believed to be the source of tumorigenesis [21].

Using single cell RNA-sequencing, we identified seven clusters in the WT and BR MM.1S cells by analyzing the transcriptome, among them cluster 2, 5, and 6 were mainly from WT cells, and cluster 0, 1, 3, and 4 from BR cells (Fig. 1f). We used the Monocle assay to order single cells

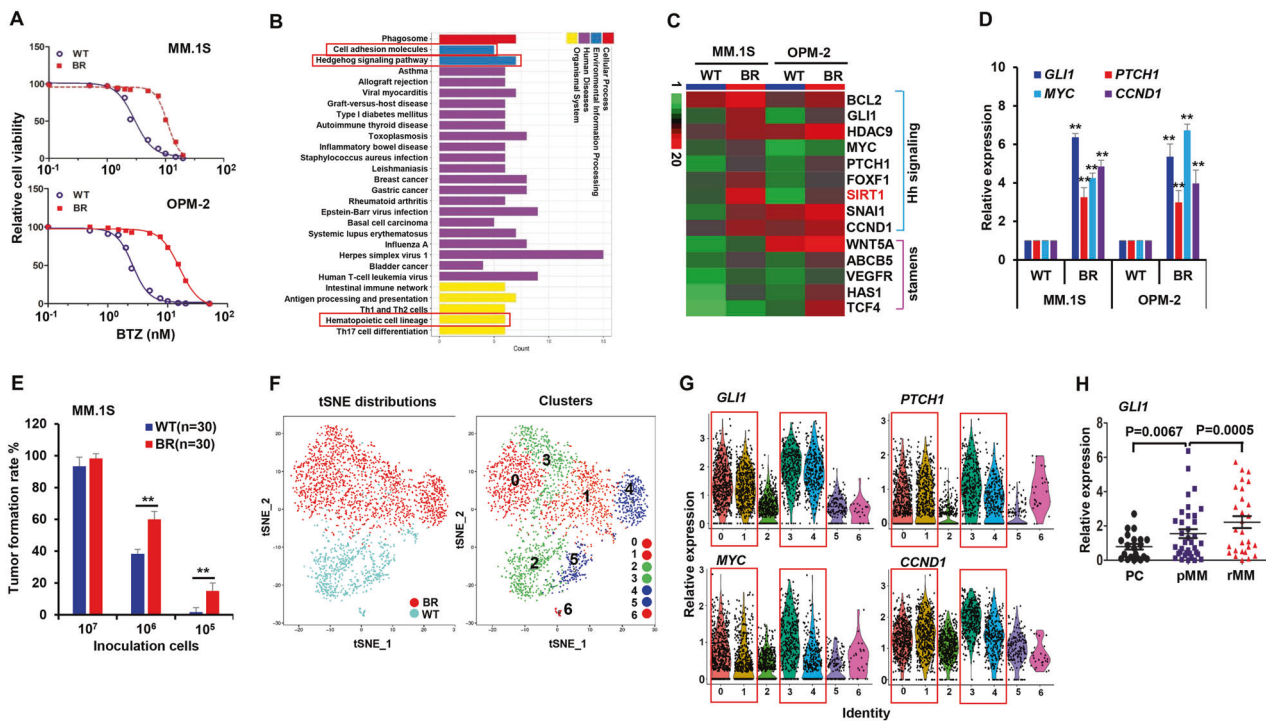


Fig. 1 The Hedgehog signaling pathway was highly activated in the bortezomib-resistant myeloma cells. **a** IC₅₀ of bortezomib in the wild type (WT) and bortezomib-resistant (BR) MM.1S and OPM-2 cells. **b** KEGG analysis highlighted the cell adhesion molecules, hedgehog signaling pathway, and hematopoietic cell lineage alternation in the BR MM cells. **c** Heat map showed the hedgehog signaling target genes and cancer stem cell related genes expressions (fold change) in the WT and BR MM.1S and OPM-2 cells. **d** Shown are real-time PCR results to confirm the activation of hedgehog signaling by the target genes *GLII*, *PTCHI*, *MYC*, and *CCND1* expressions. **e** The tumor formation assay for WT and BR MM.1S by inoculation of 1×10^7 , 1×10^6 , and

1×10^5 cells on the flanking of NSG/SCID mice for 4 weeks. $**p < 0.01$ compared with the WT controls. Single cell RNA-sequencing for 3916 WT and 4179 BR MM.1s cells divided cells into seven clusters according to different transcriptome characteristics by the t-SNE (t-distributed stochastic neighbor embedding) plot method. **g** Expressions of Hh signaling target genes, *GLII*, *PTCHI*, *MYC*, and *CCND1* in different clusters indicated higher expression level in the cluster 0, 1, 3, and 4 from BR MM.1S cells. **h** *GLII* mRNA level in plasma cell (PC) from 21 healthy donors, CD138⁺ cells from 38 newly diagnosed and 28 relapsed myeloma patients

and construct the differentiation trajectory with a tree-like structure, and confirmed that clusters 0, 1, 3, and 4 were traced with the BR trajectory (data not shown). We also confirmed that gene expression patterns of *GLII*, *PTCHI*, *MYC*, and *CCND1* in different clusters, and found they are highly expressed in the cluster 0, 1, 3, and 4, which were all from BR MM.1S cells (Fig. 1g). Clinically, we examined B cells from 21 healthy donors, and CD138⁺ cells from 38 newly diagnosed and 28 relapsed myeloma patients, and found *GLII* expression was significantly elevated in the newly diagnosed myeloma patients ($P < 0.05$), and even higher in the relapsed myeloma patients ($P < 0.001$), suggesting the activation of Hh signaling in MM patients (Fig. 1h).

SIRT1 level is associated with bortezomib resistance in myeloma cells

Intriguingly, we found that *SIRT1* was highly expressed along with Hh signaling targets in the BR MM cells, and sought to investigate the roles and regulation mechanism.

We firstly examined the expressions of all class III HDACs, and confirmed *SIRT1* expression was the most prominent among all seven members (Fig. 2a). Besides, the *SIRT1* protein was also elevated gradually during the induction of drug resistance (Fig. 2b, Supplementary Fig. 1A), and the dose- and time-dependent manners of *SIRT1* expression was elicited both in the MM.1S and OPM-2 cells (Supplementary Fig. 2b), as well as other MM cells like RPMI8228, LP-1, H929, and U266 cells (Supplementary Figs. 1C, 2D). Intriguingly, carfilzomib treatment also invoked the *SIRT1* expression (Supplementary Figs. 1E, 2F), but dexamethasone and melphalan failed to upregulate *SIRT1* expression in MM.1S and OPM-2 cells (Supplementary Figs. 1G, 2H), indicating the *SIRT1* overexpression may be proteasome inhibitor specific. In CD138⁺ plasma cells isolated from myeloma patients, we found the *SIRT1* expression was significantly elevated in the newly diagnosed patients but even higher in the relapsed patients treated with bortezomib-based therapeutic regimens (Fig. 2c), and the protein level of *SIRT1* was also been validated in the bone marrow tissues of myeloma patients

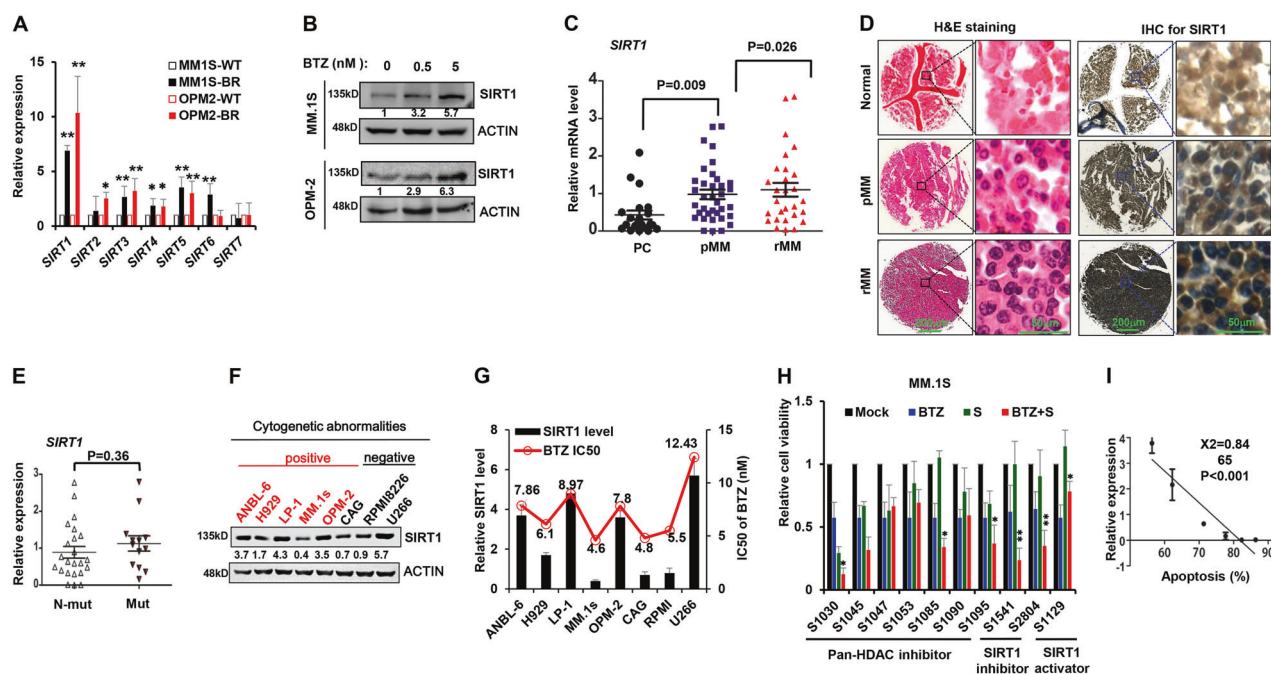


Fig. 2 SIRT1 expression is correlated with bortezomib resistance in myeloma cells. **a** qPCR to detect the expressions of all class III HDAC family genes in WT and BR MM.1S and OPM-2 cells. **b** Protein level of SIRT1 during the induction of BTZ-resistant MM.1S and OPM-2 cells. **c** *SIRT1* mRNA level in plasma cell (PC) from 21 healthy donors, CD138⁺ cells from 38 newly diagnosed and 28 relapsed myeloma patients. **d** Representative H&E staining and immunohistochemical staining for SIRT1 protein in the sequential bone tissue slides from healthy donor, newly diagnosed and refractory myeloma patients. Magnification: left panel, 4 \times ; right panel, 400 \times . **e** *SIRT1* mRNA level in CD138⁺ cells from 13 myeloma patients with RAS/RAF mutations and 23 myeloma patients without mutations. **f** SIRT1 levels in eight myeloma cell lines with (red labels, positive) or without (black label, negative) cytogenetic abnormalities (red labels), and **g** showed the

individual IC₅₀ of bortezomib in these cells along with the relative SIRT1 protein levels referred to the ACTIN level. Red cell lines, myeloma cells with t(14;16)(q13,q32) or t(14, 16)(p16,q32) translocation mutations; black cell lines, no mutations reported. **h** Combination treatment of bortezomib with HDAC inhibitors or activators from an epigenetic compound library in MM.1S cells and OPM-2 cells to evaluate the synergetic anti-MM effects. **i** Correlation of *SIRT1* level and sensitivity to bortezomib in CD138⁺ cells from six myeloma patients using the flow cytometry assay. All data represent results from at least three independent experiments, numbers under the western blots are relative levels compared with the mock control or to the density of ACTIN according to gray scale densities. * $p < 0.05$; ** $p < 0.01$

(Fig. 2d, Supplementary Fig. 2A, B). However, we did not find any difference of *SIRT1* expressions in CD138⁺ plasma cells from the patients with or without RAS/RAF mutations (Fig. 2e). We also detected the endogenous levels of SIRT1 in eight myeloma cell lines, and found the SIRT1 levels varied largely, but no significant correlations were found with the cytogenetics background, such as t(14;16)(q32;q23) or t(4;14)(p16;q32) abnormalities (Fig. 2f, Supplementary Fig. 3A); in addition, myeloma cells with higher SIRT1 expression had higher half maximal inhibitory concentration (IC₅₀) to bortezomib, and the difference was obvious (Fig. 2g). These data suggested that elevated SIRT1 expression had positive correlation with proteasome inhibitor.

To further elucidate the functions of SIRT1 in anti-MM effect of bortezomib, we screened an epigenetic compound library including 182 compounds with bortezomib, and identified the SIRT1 inhibitor S1541 (EX527, Selisistat) and S2804 (Sirtinol) had very obvious synergetic anti-myeloma effect, but SIRT1 activator SRT1129 antagonized

the antimyeloma effect of bortezomib remarkably (Fig. 2h, Supplementary Fig. 3B). Importantly, these chemicals exert their functions without obvious solo cytotoxicity even at 10 \times and 100 \times IC₅₀ dosage both for MM.1S and OPM-2 cells (Supplementary Fig. 3C, D). When the SIRT1 gene was manipulated using lentivirus carrying either pTA-SIRT1-flag (SIRT1-OE), CRISPR/cas9 sgRNA targeting SIRT1 (SIRT1-KD), significant lower apoptosis rate was elicited in the SIRT1-OE myeloma cells compared with the vector control, and vice versa in the SIRT1-KD myeloma cells (Supplementary Fig. 3E). The combined antimyeloma effect of manipulating SIRT1 together with bortezomib was also confirmed by detecting the cleavage of PARP by western blotting (Supplementary Fig. 3F). Clinically, when we analyzed CD138⁺ plasma cells from six myeloma patients, a negative correlation between SIRT1 expression and apoptosis rate induced by 5 nM bortezomib could be derived (Fig. 2i). These results further supported a crucial role of SIRT1 in mediating bortezomib sensitivity for MM cells.

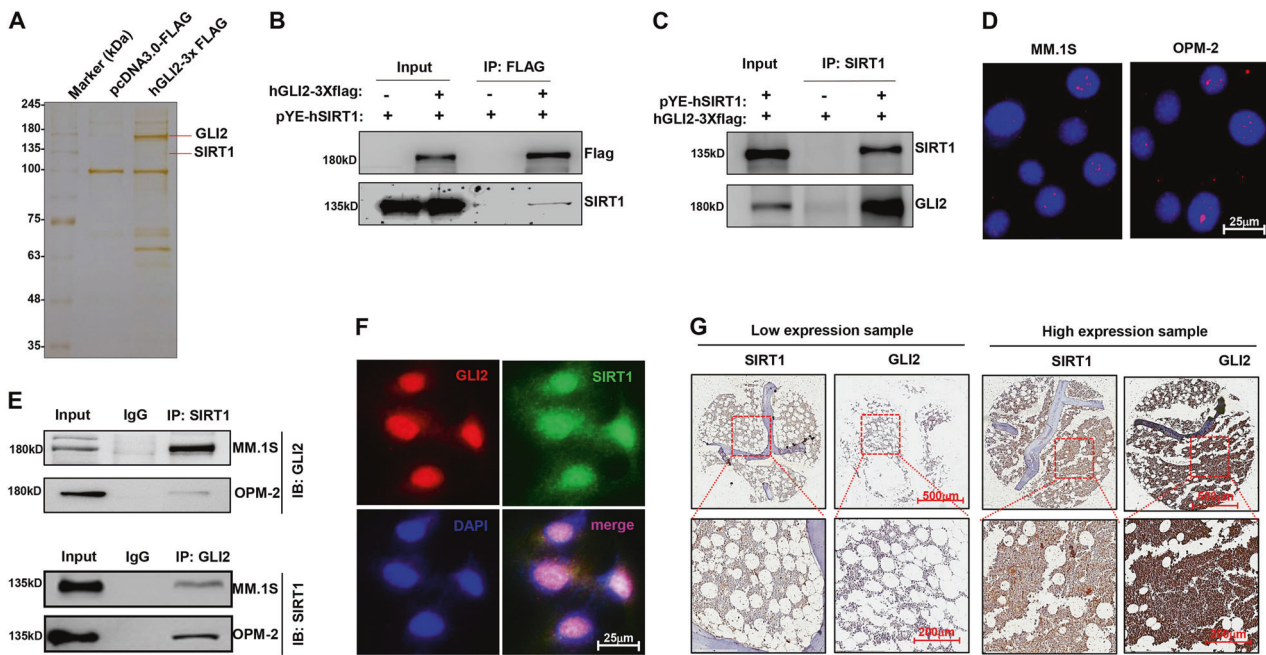


Fig. 3 SIRT1 physically interacts with GLI2 in myeloma. **a** Silver staining for flag-pulldown in HEK293T cells transfected with pcDNA3-3 × flag or pcDNA3-3 × flag-GLI2 for 48 h. **b** Co-immunoprecipitation (Co-IP) to detect the interaction between exogenous GLI2 and SIRT1 in HEK293T cells transfected with pcDNA3-3 × flag-GLI2 and pYE-SIRT1 for 48 h, and **c** reversely immunoprecipitated exogenous SIRT1 and immunoblotted with GLI2. **d** Detection of protein–protein interaction using the proximity ligation assay (PLA) in NIH/3T3 cells. **e** Endogenous GLI2 and SIRT1 interaction in MM.1S cells and OPM-2 cells using GLI2 antibody or reversely SIRT1 antibody for immunoprecipitation. **f** Immunofluorescence staining of GLI2 (555-conjugated) and SIRT1 (FITC-conjugated) in MM.1S cells to show the subcellular co-localization. **g** Immunohistochemical staining of GLI2 and SIRT1 proteins in the sequential bone marrow slides from the same myeloma patients to show the correlation of expression. Magnifications: upper, 4×; lower, 20×

(PLA) in NIH/3T3 cells. **e** Endogenous GLI2 and SIRT1 interaction in MM.1S cells and OPM-2 cells using GLI2 antibody or reversely SIRT1 antibody for immunoprecipitation. **f** Immunofluorescence staining of GLI2 (555-conjugated) and SIRT1 (FITC-conjugated) in MM.1S cells to show the subcellular co-localization. **g** Immunohistochemical staining of GLI2 and SIRT1 proteins in the sequential bone marrow slides from the same myeloma patients to show the correlation of expression. Magnifications: upper, 4×; lower, 20×

SIRT1 directly interacts and deacetylates GLI2 protein at lysine 757 to enhance Hh signaling activation

Since SIRT1 expression is associated with activation of the Hh signaling pathway, we then investigated whether it plays the functional role through the most important transcriptional factor GLI2 of Hh signaling. We ectopically expressed the SIRT1-flag protein in HEK293T cells for the mass spectrum assay after immunoprecipitation, and found SIRT1 was one of the components of GLI2 complex (Fig. 3a). Accordingly, we immunoprecipitated the GLI2 or SIRT1 protein respectively to determine the protein–protein interaction, and found they could combine each other (Fig. 3b, c). Remarkably, interaction between endogenous SIRT1 and GLI2 was also validated by in situ proximity ligation (Fig. 3d, Supplementary Fig. 4A) and immunoprecipitation assays in myeloma cells (Fig. 3e). Our result also demonstrated that the interaction intensity with GLI2 had no obvious differences in MM.1S and MM.1R cells, indicating dexamethasone resistance does not affect SIRT1 (Supplementary Fig. 4B) [22]. Immunofluorescence staining for SIRT1 and GLI2 proteins indicated SIRT1 and GLI2 were mainly co-localized in the nucleus of MM cells (Fig. 3f), and immunohistochemistry

staining in serial bone marrow tissue sections from the same patient indicated a highly positive expression correlation (Fig. 3g, Supplementary Fig. 4C, D). These findings uphold a direct clue for modification of GLI2 protein by SIRT1 to activate the Hh pathway.

To determine whether SIRT1 modifies GLI2 transcriptional activity, we transfected an 8 × GLI luciferase reporter together with different titers of pITA-SIRT1 lentivirus, and found that ascending SIRT1 increased GLI transcriptional activity at a dose-dependent manner (Fig. 4a), under the condition that SIRT1 expression gradually elevated according to the virus titers (Supplementary Fig. 5A). When SIRT1 expression was exogenetically manipulated, or the SIRT1 activity was pharmacologically disturbed by the activator SRT1720 or inhibitor EX527, the GLI2 protein level could be elevated or suppressed, respectively (Fig. 4b, c). At the same time, mRNA of Hh signaling target genes, the *PTCH1*, *GLI1*, *CCND1*, were all consequentially altered according to the SIRT1-OE or SIRT1-KD, respectively (Supplementary Fig. 5B, C). When SIRT1 expression was ectopically altered in NIH3T3 cells, majority of GLI2 were translocated from cytoplasm to nucleus with SIRT1 overexpression, but retained in the cytoplasm in the SIRT1 knockdown cells (Fig. 4d, Supplementary Fig. 5D), and the subcellular fractionation assay for GLI2 also confirmed the

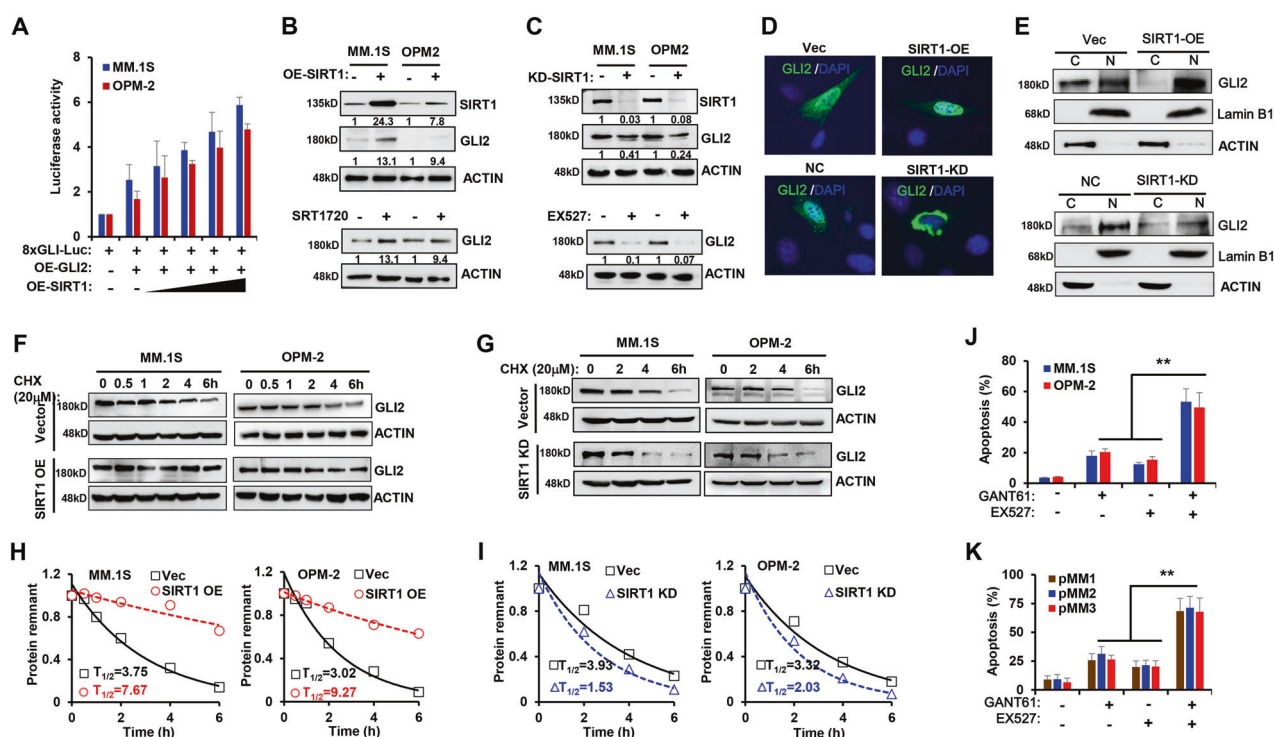


Fig. 4 SIRT1 activates hedgehog signaling via stabilizing GLI2 protein. **a** The luciferase assay of $8 \times$ GLI-reporter in MM.1S and OPM-2 myeloma cells electroporated with $3 \times$ FLAG-GLI2 ($1 \mu\text{g}$) and increasing ratios of pTA-SIRT1 lentivirus. **b** MM.1S and OPM-2 cells infected with lentivirus carrying pTA-SIRT1 plasmid for 72 h (upper panel), or treated with $0.5 \mu\text{M}$ SIRT1720 (SIRT1 activator) for 48 h, and the GLI2 protein were detected using the western blotting assay. **c** MM.1S and OPM-2 cells infected with lentivirus carrying CRISPR/cas9-SIRT1 sgRNA for 72 h, or treated with $2.5 \mu\text{M}$ EX527 (SIRT1 inhibitor) for 48 h, and the GLI2 protein were detected using the western blotting assay. **d** The immunofluorescence assay to detect the translocation of GLI2 protein in NIH/3T3 cells with SIRT1 overexpression (OE) or knockdown (KD), compared with vector control (Vec) or nontarget control (NC) respectively. Magnification, $600 \times$. **e**

Cytoplasmic and nuclear fraction of GLI2 in NIH/3T3 cells with SIRT1-OE or KD compared with Vec or NC controls respectively were detected using western blotting. **f** MM.1S and OPM-2 cells were infected with lentivirus expressing pTA-SIRT1 plasmid or **g** CRISPR/cas9-SIRT1 for 72 h, and degradation of GLI2 protein within 6 h with the presence of $20 \mu\text{M}$ cycloheximide was monitored using the western blotting assay. **h**, **i** showed the calculated half-life of GLI2 protein in the above myeloma cells. **j** Synergetic antimyeloma effect of GLI inhibitor GANT61 and SIRT1 inhibitor EX527 was evaluated using flow cytometry in MM.1S and OPM-2 cells, and **k** CD138⁺ cells from three myeloma patients. All data represent results from at least three independent experiments, numbers under the western blots are relative levels compared with the mock control or to the density of ACTIN according to gray scale densities. ****** $p < 0.01$

translocation from cytoplasm to nuclear in MM.1S cells (Fig. 4e).

We next evaluated whether SIRT1 can protect GLI2 protein from degradation. As predicted, GLI2 protein accumulated gradually with the SIRT1 activator SIRT1720 treatment (Supplementary Fig. 5E), and attenuated progressively with the SIRT1 inhibitor EX527 treatment (Supplementary Fig. 5F), both at a dose-dependent manner. In addition, the GLI2 degradation was significantly postponed according to SIRT1 overexpression (Fig. 4f), and accelerated for SIRT1 knockdown (Fig. 4g) in MM.1S and OPM-2 cells respectively, since the half-life of GLI2 protein was augmented almost threefold (Fig. 4h) and receded over two times (Fig. 4i). Furthermore, pharmacological inhibition of SIRT1 and Hh signaling induced obvious synergetic apoptosis both in two myeloma cell lines (Fig. 4j), and in CD138⁺ plasma cells from three patients (Fig. 4k). These

results strongly suggest that SIRT1 regulate Hh signaling activation through modulating the key transcriptional factor GLI2.

Previous study had revealed that mouse Gli could be deacetylated by HDAC1 [16], therefore we proposed human GLI2 protein could also be deacetylated. Indeed, when exogenous GLI2 in HEK293T cells were immunoprecipitated and immunoblotted with anti-acetylated lysine, we found GLI2 were constitutively acetylated (Fig. 5a), and its acetylation could be enhanced by co-transfection of p300-HA (Fig. 5b) or reverted by overexpression of pYE-SIRT1 (Fig. 5c). Since both the acetylation of Ci in *Drosophila* and Gli in mammalian have been proved to link ubiquitination for degradation [17], we verified whether SIRT1 could affect the ubiquitination-mediated degradation of GLI2. Our results clearly showed SIRT1 overexpression attenuated, but overexpression of p300 enhanced the GLI2

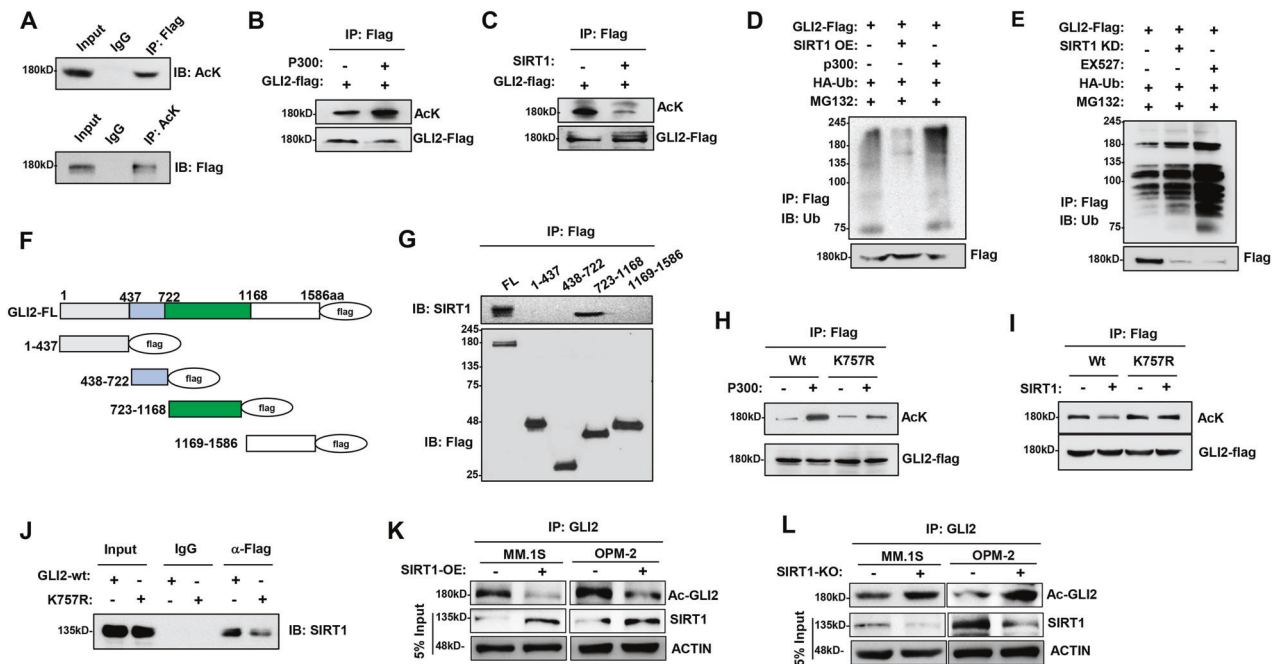


Fig. 5 SIRT1 deacetylates GLI2 at K757 and suppresses its ubiquitination. **a** HEK293T cells were transfected with pcDNA3-3 × flag-GLI2 for 48 h, after flag (upper lanes), acetylated lysine (lower lanes), or IgG control immunoprecipitation, acetylation status of GLI2 were detected by anti-acetylated lysine (upper lanes) and anti-flag (lower lanes). HEK293T cells were transfected with pcDNA3-3 × flag-GLI2 together with **b** P300 or **c** SIRT1 for 48 h, after flag or IgG control immunoprecipitation, the acetylation status of GLI2 were detected by anti-acetylated lysine. HEK293T cells were transfected with pcDNA3-3 × flag-GLI2 for 48 h, with SIRT1 overexpression (**d**) or SIRT1 inhibition (**e**), either by expressing plasmids or inhibitor for 48 h, and after flag immunoprecipitation, the ubiquitination status of GLI2 was

detected by ubiquitin antibody. Truncations design for GLI2 full length protein (**f**) and expression and interactions with SIRT1 in HEK293T cells by flag immunoprecipitation. GLI2⁷³²⁻¹¹⁶⁸ was mutated at K757 and transfected into HEK293T cells together with **h** P300 or **i** SIRT1, and the acetylation status of truncation was detected using flag immunoprecipitation and anti-acetylated lysine immunoblotting, and **j** interaction capability with SIRT1 was evaluated. GLI2 acetylation status in MM.1S and OPM-2 cells with **k** SIRT1 overexpression or **l** knockdown by CRISPR/cas9 sgRNA were detected using GLI2 immunoprecipitation and anti-acetylated lysine immunoblotting. For all immunoprecipitation, 5% input was loaded as control, and all data represent at least three independent experiments

ubiquitination obviously (Fig. 5d); on the contrary, when SIRT1 abrogation was achieved pharmacologically or by CRISPR/cas9 sgRNA, the GLI2 ubiquitination was remarkably enhanced (Fig. 5e). To map the acetylated residues of GLI2 by SIRT1, we designed GLI2-truncations for flag-pulldown (Fig. 5f). When these truncations were expressed and flag-immunoprecipitated, we found only the GLI2^{full length} and GLI⁷²³⁻¹¹⁶⁸ truncation could interact with SIRT1 protein (Fig. 5g). According to a KAT-specific acetylation sites database and prediction, there were six potential KAT sites, but when these lysines were mutated to arginine, only the mutation of K757 altered the acetylation status of GLI2 modified by p300 (Fig. 5h) and SIRT1 (Fig. 5i). Moreover, mutation at K757 also attenuated the interaction intensity of GLI2 with SIRT1 (Fig. 5j). Remarkably, when SIRT1 was overexpressed or knockdown in myeloma cells, the acetylation of endogenous GLI2 was also diminished or enhanced accordingly (Fig. 5k, l). Overall, these findings strongly suggested that SIRT1 deacetylates GLI2 protein at K757 residue on the C-terminus containing transcriptional active motif.

SIRT1 is a direct target of Hh signaling

Given *SIRT1* expression is correlated with Hh activation, we suppose that *SIRT1* itself may be a direct target of Hh signaling. To verify this hypothesis, we constructed a 1287 kb (−1241 to +46 bp) promoter of *SIRT1* gene onto a pGL3-basic vector, and transfected it into HEK293T cells together with GLI2 expressing plasmid, to examine the transcriptional activity of *SIRT1* gene. The luciferase assay indicated that *SIRT1* transcriptional activity was gradually stimulated by GLI2 protein (Fig. 6a), which was also reflected by *SIRT1* mRNA level (Supplementary Fig. 6A) and protein level (Fig. 6b). In addition, we treated the NIH/3T3 cells with recombination mouse Shh-N peptide for 24 h to activate Hh signaling, and found that both the *Sirt1* mRNA (Supplementary Fig. 6B) and *Sirt1* protein (Supplementary Fig. 6C) were upregulated gradually. Through bioinformatics analysis, we found there are four GLI binding sites on the *SIRT1* promoter, and binding of GLI2 transcriptional factor on these DNA fragments were all confirmed by the chromatin immunoprecipitation (ChIP)

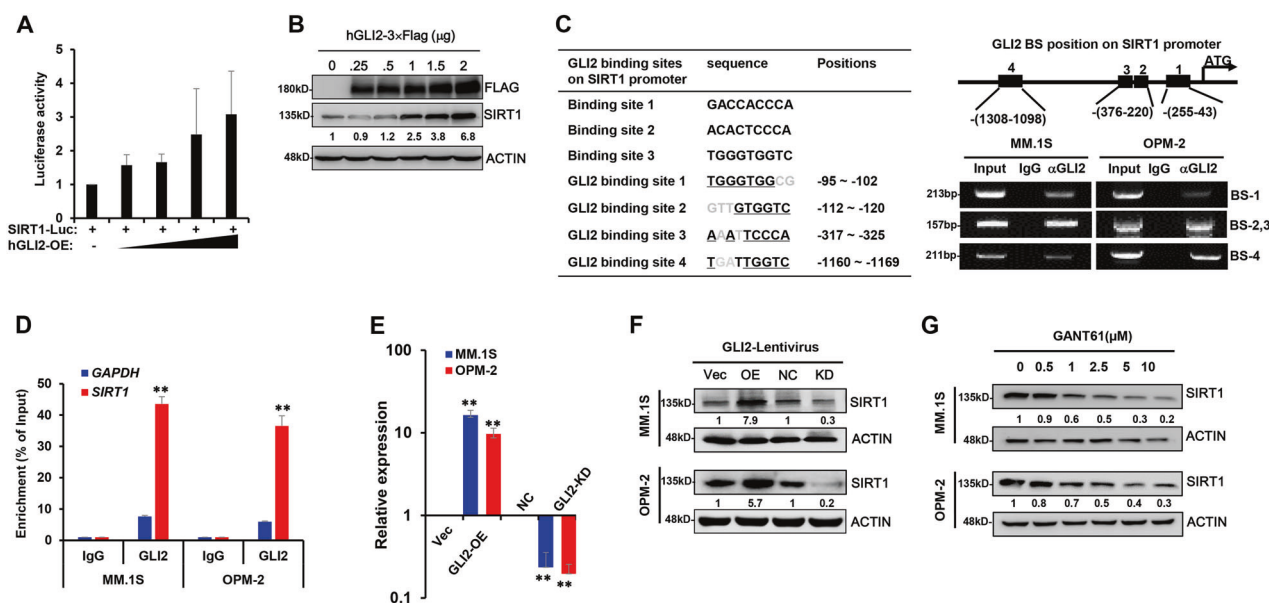


Fig. 6 *SIRT1* is a direct target of hedgehog signaling. **a** The luciferase assay of hSIRT1-promoter (SIRT1-pro) in HEK293T cells transfected with increasing amount of pcDNA3-3 × FLAG-GLI2 plasmid. **b** The western blotting assay showed the protein level of SIRT1 due to 3 × flag-GLI2 overexpression in HEK293T cells. **c** GLI2 binding sites, sequences and positions on the SIRT1 promoter (left panel), and ChIP-PCR to detect the GLI2 binding sites (BS) on the SIRT1 promoter in MM.1S and OPM-2 cells (right panel). **d** The enrichment of GLI2 on the promoter regions of *SIRT1* was confirmed by real-time PCR using the ChIP products. **e** Real-time PCR to detect the *SIRT1* mRNA levels

and **f** western blotting showed the SIRT1 protein level in MM.1S or OPM-2 myeloma cells infected with GLI2 overexpression (OE) or knockdown with CRISPR/cas9 sgRNA lentivirus (KD). ** $p < 0.01$. **g** SIRT1 protein in MM.1S and OPM-2 cells treated with GLI inhibitor GANT61 (0–10 μM) for 24 h was detected by western blotting. All data represent results from at least three independent experiments, numbers under the western blots are relative levels compared with the mock control or to the density of ACTIN according to gray scale densities

assay (Fig. 6c), and the recruitment of GLI2 onto the *SIRT1* promoter was significantly abundant compared with that on *GAPDH* promoter using ChIP-qPCR, indicating the binding of GLI2 on SIRT1 promoter is specific (Fig. 6d). Furthermore, when GLI2 was ectopically manipulated in myeloma cells, both the *SIRT1* mRNA (Fig. 6e) and protein level (Fig. 6f) were up- or downregulated accordingly. Similarly, pharmacological suppression of GLI2 in myeloma cells resulted in the downregulation of SIRT1 (Fig. 6g), demonstrating that the Hh-mediated regulation of SIRT1 was functionally relevant. These data suggested the existence of a SIRT1-GLI2-Hh signaling-SIRT1 positive regulatory loop in myeloma.

Targeting SIRT1 synergistically enhanced sensitivity to bortezomib treatment for MM cells in vitro and in vivo

Finally, we aimed to clarify the significance of targeting SIRT1 in overcoming bortezomib resistance in myeloma. BTZ treatment triggered limited apoptotic portions of BTZ-BR MM.1S and OPM-2 cells compared with their WT controls, but surprising improvement of antimyeloma effect was induced when the EX527 was in present (Fig. 7a), and this synergetic antimyeloma consequence could also be

verified by the cleavages of PARP (Fig. 7b). Notably, NOD/SCID mice bearing BTZ-BR MM.1S and OPM-2 cells in a xenograft model showed that when mice were treated with bortezomib and EX527 collaboratively, tumor growth was remarkably suppressed compared with individual administration of BTZ or EX527 (Fig. 7c, d), and the overall survival of mice was significantly prolonged (Supplementary Fig. 7A, B). At the same time, BTZ-BR myeloma cells were injected into the femur bone marrow of NOD/SCID mice for bone lesion evaluation. Our data clearly showed significant remission of bone lesion in the BTZ plus EX527 group compared with the vehicle control, BTZ or EX527 alone groups (Fig. 7e), and there was a significant decrease in lesion area in the combination group compared with the vehicle, BTZ or EX527 alone groups (Fig. 7f). Importantly, when we collected clinical samples from 39 myeloma patients with detailed follow-up information, then divided them into two groups according to the median value of *SIRT1* mRNA level, we found high *SIRT1* expression correlated with worse survival tendency in myeloma patients under bortezomib-based therapy regimen (Fig. 7g). Among these patients, we had collected samples from 2 MM patients with complete response (CR) and three patients with relapsed MM, and the consecutive monitor of SIRT1 expression in CD138+ plasma cells indicated that *SIRT1*

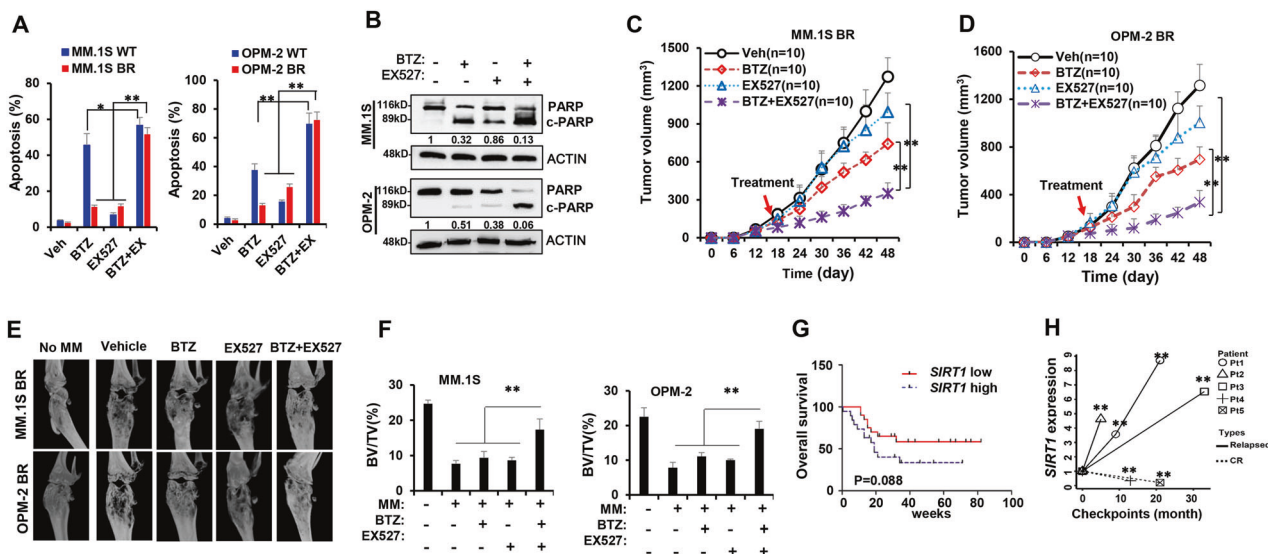


Fig. 7 Synergetic antimyeloma effect of bortezomib and SIRT1 inhibitor in vitro and in vivo. **a** Shown are apoptosis rates of WT and BR MM.1S and OPM-2 cells treated with 5 nM of BTZ in presence or absence of 5 μM EX527 for 48 h analyzed by flow cytometry, and **b** the cleavage of PARP by western blot. NOD/SCID mice bearing **c** BR MM.1S cells and **d** BR OPM-2 cells were injected into the left flanking of mice and treated with 0.5 mg/Kg bortezomib with or without 0.5 mg/Kg EX527 from day 12 to day 48, and tumor volumes were monitored every 3 days as $1/2(L \times W^2)$ mm, where the L presenting the length and W representing width of tumor. **e** MM.1S and OPM-2 BR cells were injected into bone marrow of NOD/SCID mice ($n = 5$) and treated with 0.5 mg/Kg bortezomib with or without 0.5 mg/

kg EX527 for 2 months, the bone lesion status were monitored by microCT scan, and **f** the bone volume per trabecular volume (BV/TV) was calculated. **g** Thirty-nine myeloma patients were divided into two groups (*SIRT1* low vs *SIRT1* high) by the median of *SIRT1* mRNA value, and the overall survival rate was analyzed using Kaplan–Meier Survival Analysis. **h** CD138+ myeloma cells from three relapsed patients and two complete response (CR) patients were collected at different treatment times and the *SIRT1* expression was detected using real-time PRC. All data represent results from at least three independent experiments, numbers under the western blots are relative levels of total PARP compared with the mock control according to gray scale densities. * $p < 0.05$; ** $p < 0.01$

expression were elevated in all relapsed patients, but suppressed in the CR patients (Fig. 7h). Overall, these data coherently suggest that targeting *SIRT1* contributed to overcome BTZ-resistance of myeloma cells in vitro and in vivo.

Discussion

In the current study we reported that SIRT1, but not other HDACs, played the most critical role in proteasome inhibitor induced chemoresistance in MM. Our study also suggested that elevated SIRT1 could be used as a hallmark for monitoring the appearance of PIs induced chemoresistance in myeloma, because its expression pattern was consistent in BR myeloma cells and in clinical patients treated with bortezomib-based treatment regimens, but independent of somatic mutations or cytogenetic abnormalities. Importantly, SIRT1 expression negatively correlated with clinical outcomes, and interference of SIRT1 impaired PIs induced drug resistance in myeloma.

Despite considerable advancements in myeloma management, the acquisition of drug resistance is becoming a major obstacle of myeloma therapy. To overcome drug

resistance, there is of the utmost importance to understand the mechanisms underlying bortezomib resistance. Our previous studies disclosed that autocrine sonic Hh activated canonical and MAPK-induced GLI2-mediated non-canonical Hh signaling contribute to the drug resistance in myeloma [6, 7], as well as the activation of autophagy in myeloma cells by adipocyte secreted adipokines [23]. In our study, we screened gene expression profiles in two BR myeloma cell lines and found 286 highly upregulated and 75 significantly downregulated genes using RNA-sequencing, and part of these dysregulated genes are Hh signaling, cancer stem cell, and hematopoietic cell lineage related. This is unsurprising because Hh signaling is closely related to cancer stem cells, and the later have been widely reported to contribute to chemoresistance in varies of cancers [24, 25]. To clarify the heterogeneity in the BTZ-resistant MM cells, we also employed single cell RNA-sequencing technique in the WT and BR-resistant MM.1S cells. According to different transcriptome characteristics, we identified seven clusters in these cells, whose transcriptional features have been obviously altered, and we confirmed that some targets of Hh signaling, such as *GLI1*, *PTCHI*, *MYC*, and *CCND1* are obviously upregulated in clusters originated from BR cells than those from WT cells. Our study

Table 1 Characteristics of patients enrolled in this study

Characteristic	No. of patients (<i>n</i> = 66)
Median Age (range)	68 (51–85)
Gender	
Male	44 (64.7%)
Female	24 (35.3%)
Diagnosis	
New diagnosed	38 (57.6%)
Relapsed	28 (42.4%)
Stage	
I	16 (24.2%)
II	17 (25.8%)
III	23 (34.8%)
Not determined	10 (15.2%)
Mutation types	
RAS/RAF	13 (19.7%)
Chromosomal anomaly	15 (22.7%)
NA	38 (57.6%)
Therapy regimen	
VD	6 (21.4%)
PCD	12 (42.8%)
PAD	10 (35.8%)

RAS/RAF mutations includes BRAF V600, KRAS G12/G13, NRAS G12/G13, and NRAS Q61 mutations. Chromosomal abnormalities include t(4;14), 1q+, 13q-, t(14;16), t(14;20), 17p- (tp53-). Regimens: PD, bortezomib + dexamethasone; PCD, bortezomib + dexamethasone + cyclophosphamide; PTD, bortezomib + dexamethasone + thalidomide

NA negative or not applicable

suggests that after bortezomib induction, certain populations in the MM cells smartly transformed to stem-like cells via alternation of Hh signaling.

Our study also elaborated the detailed molecular mechanism of SIRT1 in regulating the key transcriptional factor GLI2. Posttranslational modifications such as phosphorylation, ubiquitination, and acetylation, play crucial roles in modulating the stabilization, DNA binding capability, and transcriptional activity of GLI proteins [17, 26]. In mammals, the GLI family transcription factors, GLI1, GLI2, and GLI3, all have conserved DNA-binding domains with five tandem C2H2 zinc fingers and recognize the consensus sequence GACCACCCA and TGGGTGGTC of the genome [27]. Among GLI families, GLI2 is the first responder following the binding of Hh ligand to the receptor and the strongest activator for Hh signaling output, whereas GLI1 most likely serves as a signal amplifier downstream of GLI2, but GLI3 is the strongest repressor. Based on the prediction of acetylation modification on the GLI2 protein through open accessed websites, we hypothesized that SIRT1 may deacetylate GLI2 to alter the protein stability and transcriptional activity. By immunoprecipitation of

GLI2 protein and the mass spectrum assay, we identified that SIRT1 was a components of the GLI2 complex, but did not find other HDACs in myeloma cells as reported in mouse Gli proteins [17]. The direct interaction of SIRT1 results in deacetylation of GLI2 at K757 residue, and consequentially alleviates the proteasome-dependent degradation via the polyubiquitination modified pathway. Remarkably, we found the acetylated-K757 site in human GLI2 has the same KLPL motif as reported in mouse Gli [16]. Intriguingly, we propose SIRT1 as the direct target of Hh signaling, because at least four GLI binding sites featured by consensus binding site AACTCCCA or TGGGTGGTC on the *SIRT1* promoter was identified. To the best of our knowledge, this is the first report of SIRT1 as the downstream target of the Hh signaling pathway. Thus, our data revealed an important positive regulating loop between SIRT1 and GLI2 in acquired drug resistance in myeloma.

Our study further emphasized the importance of SIRT1 among all HDACs in drug resistance to bortezomib in myeloma cells, both by bench work and clinical analysis. Our results indicate that upregulation of SIRT1 is PIs specific, because the both bortezomib and carfilzomib induced SIRT1 expression, but other anti-MM agents, such like melphalan and dexamethasone failed to provoke the dysregulation of SIRT1. Moreover, we did not find any combining capacity difference between SIRT1 and GLI2 proteins in the MM.1S and MM.1R cells, in which the MM.1R is a well-known dexamethasone-resistant MM cells generated from MM.1S [22]. Although some other HDACs, such as HDAC3, HDAC-4 have been reported to play important roles in myeloma tumorigenesis [28, 29], only SIRT1 has been reported to do with BR in myeloma, probably through increasing the ROS, decreasing in VEGF-induced migration and angiogenesis, as well as abrogation of the NF- κ B signaling pathway [18], but did not concerning the cancer stem cell and Hh signaling. Although we found dysregulation of some other HDAC genes, but only confirmed the direct interaction of SIRT1 and GLI2. The reason we want to highlight SIRT1 is that, at least partially, metabolism alternations but not Zn²⁺ concentration are often found in cancers, since class III HDACs are NAD⁺-dependent deacetylases, whereas other classes of HDACs exert their functions via Zn²⁺-dependent deacetylation [14, 30]. Thus, the significance of our study is to clarify the applications of HDAC inhibitors in overcoming the relapsed or refractory patients with myeloma, therefore reduce the side effects of the pan-HDAC inhibitors and achieve better outcomes for myeloma patients.

Overall, our results indicate that the SIRT1 is a mutation-independent and proteasome inhibitor specific key regulator for drug resistance in myeloma, acting both as a regulator and an amplifier of the Hh signaling. The significance of our study for clinic is to develop an indicator for

chemotherapeutic response, and develop combination treatment strategies targeting SIRT1 to overcome myeloma relapse eventually.

Material and methods

Patient's samples and ethic approvals

CD138+ plasma cells were isolated from bone marrow mononuclear cells of the healthy donor, newly diagnosed or relapsed myeloma patients using CD138 MicroBeads (Miltenyi Biotec, Bergisch Gladbach, Germany) according to the manufacturer's instructions. Briefly, 3–5 ml of bone marrow biopsies were diluted up to 10 ml with RPMI-1640 media and gently loaded onto the top of 10 ml Ficoll Paque Plus (Sigma-Aldrich, St. Louis, MS, USA) and centrifuged at $800 \times g$ for 25 min at room temperature with the acceleration at 0. After centrifuge, the mononuclear cells were carefully aspirated from the Ficoll-plasma interface and washed with PBS at $300 \times g$ for 10 min at room temperature twice. For 2×10^7 total cells, the pallet was resuspended in 80 μ l buffer and labeled with 20 μ l of CD138 MicroBeads at 4 °C for 15 min. After washed, the cells were resuspended in 500 μ l buffer and proceeded for the positive selection of plasma cells from PBMC. Characteristics of patients enrolled in this study were shown in Table 1.

This study was approved by the Ethic Committee of Tianjin Medical University, all the protocols were conformed to the Ethical Guidelines of the World Medical Association Declaration of Helsinki. Signed informed consent was obtained from all participating individuals prior to participation in the study.

Cell lines and establishment of BR myeloma cells

Myeloma cell lines OPM-2, MM.1 R, and U266 were purchased from ATCC (American Type Culture Collection, Manassas, VA, USA), RPMI-8226, NCI-H929, and MM.1S from the National Infrastructure of Cell Line Resource (Beijing, China). Myeloma cells were cultured in RPMI-1640 media supplemented with 15% of fetal bovine serum, 100 U/ml of penicillin, 100 mg/ml of streptomycin, and 2 mM L-glutamine (Gibco, Life Technologies, Carlsbad, CA, USA). Cells were STR authenticated (Biowing Biotech, Shanghai, China) if cultured over 6 months and experiments were performed with mycoplasma-free cells detected with the Universal Mycoplasma Detection Kit (ATCC, Manassas, VA, USA).

To develop BR myeloma cells, parental drug-naive cells were imitated by 0.5 nM of BTZ and enhanced by doubled dosage every 1 month up to 6 months totally. Acquire of BR-resistant phenotype was monitored and confirmed by

calculating the IC_{50} of BTZ using the MTS assay. Cells with IC_{50} over ten times were kept for further experiments.

Flow cytometry and the cell proliferation assay

Flow cytometry and the cell proliferation assay have been described previously [6]. Briefly, a total of 1×10^5 cells were stained with 5 μ l Annexin V-FITC and 1 μ l of propidium iodide (PI) and analyzed by FACS Calibur instrument. Proliferation was detected using the CellTiter 96 Aqueous One Solution Reagent (Promega, Fitchburg, WN, USA), and samples were read at 490 nm with a Microplate Reader 550 (Bio-Rad Laboratories, Richmond, CA, USA). The following formula was used to calculate cell viability (%) = OD value of treatment group/OD value of control group $\times 100$.

Single cell RNA-sequencing and real-time PCR

Single cell preparation, library synthesis, RNA-sequencing and data analysis were completed by the Gene Denovo (Guangzhou, China). Briefly, 10,000 cells were counted using Countess II Automated Cell Counter and adjusted the concentration to 1000 cell/ μ l. Cells were barcode-labeled and mixed with reverse transcriptase into a Gel Beads-In-Emulsions (GEMs), then the cDNA library was amplified using PCR with the sequencing primer R1 and P5 arm, and the cDNA libraries of three independent experiments were pooled and sequenced on the Illumina 10 \times Genomics Chromium platform. Real-time PCR was performed in the QuantStudio 3 Real-Time PCR System (Applied Biosystems) as previously described [6], and primer sequences are provided in Supplementary Table 1.

Western blotting, immunohistochemistry, co-immunoprecipitation (Co-IP), and the chromatin immunoprecipitation (ChIP) assay

Western blotting was carried out as previously described [6]. All antibodies, vendors, dilutions were provided in the Supplementary materials Table 2. The representative western blot images for at least three independent experiments shown in the figures have been cropped and auto contrasted, and numbers under the blots were relative levels compared either with the control or with the ACTIN control. Co-IP and ChIP assays were referred to the previous descriptions [7], clarified lysates were precleared with Protein G-Sepharose (Pierce, Rockford, IL), and then immunoprecipitated with anti-GLI2 absorbed to protein G-Sepharose, and then blotted with anti-acetyl lysine (K) antibody (Cell Signaling Technology, Danvers, MA, USA) or anti-Ubiquitin antibody (Cell Signaling Technology, Danvers, MA, USA).

For the IHC, paraffin-embedded sections were deparaffinized and blocked, incubated with SIRT1 or GLI2 (1:200) antibody at 4 °C overnight, and then incubated with horseradish peroxidase-conjugated secondary antibody at 1:500 for 1 h at room temperature. The sections were developed using a DAB (3,3'-diaminobenzidine tetrahydrochloride) substrate kit (Thermo Scientific) at room temperature for 1–5 min and then counterstained with hematoxylin. Quantification of IHC staining intensities were analyzed using the ImageJ 1.46r software for all samples in each groups.

Luciferase assay

For the luciferase assay, 0.8 µg of total DNA including 0.2 µg 8 × GLI-Luc reporter vector and 1 ng pRL-TK Renilla plasmid as internal control, 0.2 µg pcDNA3-flag-GLI2, pYE-hSIRT1 (0.2, 0.3, and 0.5 µg), or empty pcDNA3.1-flag vectors were mixed with 1×10^6 myeloma cells in suspending buffer to the final volume of 120 µl and then electroporated using a Neon Transfection System (ThermoFisher Scientific, Waltham, MA, USA). After 48 h transfection, cell lysate was used to detect luciferase activity in a Dual-Luciferase Reporter assay system (Promega, Madison, WI, USA) according to the manufacturers' protocols, and signal captured in the SpectraMax M5 multi-detection microplate reader (Molecular Devices Corporation, Sunnyvale, CA, USA).

Immunofluorescence staining and the proximity ligation assay (PLA)

For the IF assay, myeloma cells or NIH3T3 cells were treated as described, permeabilized, and incubated with anti-GLI2 or anti-SIRT1 antibody overnight at 4 °C, samples were incubated with FITC-conjugated goat anti-mouse IgG (1:1000) for 30 min at room temperature and nucleus counterstaining with DAPI. Imaging was obtained by the Olympus IX71 fluorescence microscope (Olympus, Tokyo, Japan). For the PLA assay, the Duolink Starter kit (Sigma-Aldrich, St. Louis, MS, USA) was used according to the manufacturer's instructions. Primary antibodies were mouse anti-SIRT1 antibody (Santa Cruz Biotechnology, sc-74504, Dallas, TX, USA) and rabbit anti-GLI2 antibody (Abcam, ab26056, Cambridge, UK). Signal detection was carried out by fluorescence imaging performed using Fluoview FV3000 confocal imaging microscope (Olympus, Tokyo, Japan).

NOD/SCID xenograft and bone lesion mice models

Animal studies were approved by the Committee on Animal Research and Ethics of Tianjin Medical University, and all

protocols were confirmed to the Guidelines for Ethical Conduct in the Care and Use of Nonhuman Animals in Research. Four to six weeks old female NOD.CB17-Prkdc^{scid}/J mice (SPF Beijing Biotechnology, Beijing, China) were used to establish the xenograft ($n = 10$) and intrabone injection model ($n = 5$) as previously reported [6, 31]. The tumors volume were measured every 3 days and calculated by $(\text{length} \times \text{width}^2)/2$, and mice were blindly randomized into four groups when tumors volume reached 50 mm³, in which mice without palpable tumors were excluded. The mice femur were undergone microCT scan (Bruker micro-CT, Kontich, Belgium) as designed.

Statistical analysis

Data are shown as mean ± SD for at least three independent experiments. Differences between groups were determined using paired two-tailed Student's *t* test or Mann–Whitney nonparametric test, and two-way ANOVA plus Bonferroni post hoc test were used for all experiments. Pearson correlation test was used to determine the correlations between gene expressions, and survival analysis was done by GraphPad Prism 5.0. A *P* value less than 0.05 was considered statistically significant. * $p \leq 0.05$; ** $p \leq 0.01$, compared with the controls, respectively.

Acknowledgements This work was supported by the National Natural Science Foundation of China (81670201, 81870161, ZL), the Natural Science Foundation of Tianjin (16JCYBJC42600, ZL), the Talent Project of Tianjin Medical University (11601501/2016KJ0317, ZL), the Nanjing Key Medical Science and Technology Development Project (ZKX18023, QZ), and the Chuzhou Science and Technology Development Project (2018zd004, QZ).

Author contributions ZL and TL contributed to the design of the experiments; YX and JL contributed to writing the paper; HJ, JW, XL, JW, SZ, and JG contributed to performing the experiments and statistical analyses; YZ and QZ provided the patient samples and clinical statistics.

Compliance with ethical standards

Conflict of interest The authors declare that they have no conflict of interest.

Publisher's note Springer Nature remains neutral with regard to jurisdictional claims in published maps and institutional affiliations.

References

1. Kumar SK, Rajkumar V, Kyle RA, van Duin M, Sonneveld P, Mateos MV, et al. Multiple myeloma. *Nat Rev Dis Primers*. 2017;3:17046.
2. Avigan D, Rosenblatt J. Current treatment for multiple myeloma. *New Engl J Med*. 2014;371:961–2.
3. Robak P, Drozd I, Szemraj J, Robak T. Drug resistance in multiple myeloma. *Cancer Treat Rev*. 2018;70:199–208.

4. Wallington-Beddoe CT, Sobieraj-Teague M, Kuss BJ, Pitson SM. Resistance to proteasome inhibitors and other targeted therapies in myeloma. *Br J Haematol*. 2018;182:11–28.
5. Ok CY, Singh RR, Vega F. Aberrant activation of the hedgehog signaling pathway in malignant hematological neoplasms. *Am J Pathol*. 2012;180:2–11.
6. Liu Z, Xu J, He J, Zheng Y, Li H, Lu Y, et al. A critical role of autocrine sonic hedgehog signaling in human CD138+ myeloma cell survival and drug resistance. *Blood*. 2014;124:2061–71.
7. Liu Z, Li T, Reinhold MI, Naski MC. MEK1-RSK2 contributes to Hedgehog signaling by stabilizing GLI2 transcription factor and inhibiting ubiquitination. *Oncogene*. 2014;33:65–73.
8. Laubach JP, San-Miguel JF, Hungria V, Hou J, Moreau P, Lonial S, et al. Deacetylase inhibitors: an advance in myeloma therapy? *Expert Rev Hematol*. 2017;10:229–37.
9. Cappellacci L, Perinelli DR, Maggi F, Grifantini M, Petrelli R. Recent progress in histone deacetylase inhibitors as anticancer agents. *Curr Med Chem*. 2018;25:1.
10. Ohguchi H, Hideshima T, Anderson KC. The biological significance of histone modifiers in multiple myeloma: clinical applications. *Blood Cancer J*. 2018;8:83.
11. Yazbeck V, Shafer D, Perkins EB, Coppola D, Sokol L, Richards KL, et al. A phase II trial of bortezomib and vorinostat in mantle cell lymphoma and diffuse large B-cell lymphoma. *Clin Lymphoma Myeloma Leuk*. 2018;18:569–575. e561.
12. Wolf JL, Siegel D, Goldschmidt H, Hazell K, Bourquelot PM, Bengoudifa BR, et al. Phase II trial of the pan-deacetylase inhibitor panobinostat as a single agent in advanced relapsed/refractory multiple myeloma. *Leuk Lymphoma*. 2012;53:1820–3.
13. Islam S, Abiko Y, Uehara O, Chiba I. Sirtuin 1 and oral cancer. *Oncol Lett*. 2019;17:729–38.
14. Delcuve GP, Khan DH, Davie JR. Roles of histone deacetylases in epigenetic regulation: emerging paradigms from studies with inhibitors. *Clin Epigenetics*. 2012;4:5.
15. Simmons GE, Jr. Pruitt WM, Pruitt K. Diverse roles of SIRT1 in cancer biology and lipid metabolism. *Int J Mol Sci*. 2015;16:950–65.
16. Canettieri G, Di Marcotullio L, Greco A, Coni S, Antonucci L, Infante P, et al. Histone deacetylase and Cullin3-REN(KCTD11) ubiquitin ligase interplay regulates Hedgehog signalling through Gli acetylation. *Nat Cell Biol*. 2010;12:132–42.
17. Gulino A, Di Marcotullio L, Canettieri G, De Smaele E, Screpanti I. Hedgehog/Gli control by ubiquitination/acetylation interplay. *Vitam Horm*. 2012;88:211–27.
18. Chauhan D, Bandi M, Singh AV, Ray A, Raje N, Richardson P, et al. Preclinical evaluation of a novel SIRT1 modulator SRT1720 in multiple myeloma cells. *Br J Haematol*. 2011;155:588–98.
19. Li B, Fu J, Chen P, Ge X, Li Y, Kuitatse I, et al. The nuclear factor (erythroid-derived 2)-like 2 and proteasome maturation protein axis mediate bortezomib resistance in multiple myeloma. *J Biol Chem*. 2015;290:29854–68.
20. Armas-Lopez L, Zuniga J, Arrieta O, Avila-Moreno F. The Hedgehog-Gli pathway in embryonic development and cancer: implications for pulmonary oncology therapy. *Oncotarget*. 2017;8:60684–703.
21. Delude C. Tumorigenesis: testing ground for cancer stem cells. *Nature*. 2011;480:S43–5.
22. Chauhan D, Catley L, Hideshima T, Li G, Leblanc R, Gupta D, et al. 2-Methoxyestradiol overcomes drug resistance in multiple myeloma cells. *Blood*. 2002;100:2187–94.
23. Liu Z, Xu J, He J, Liu H, Lin P, Wan X, et al. Mature adipocytes in bone marrow protect myeloma cells against chemotherapy through autophagy activation. *Oncotarget*. 2015;6:34329–41.
24. Sari IN, Phi LTH, Jun N, Wijaya YT, Lee S, Kwon HY. Hedgehog signaling in cancer: a prospective therapeutic target for eradicating cancer stem cells. *Cells*. 2018;7:pii E208.
25. Nunes T, Hamdan D, Leboeuf C, El Bouchtaoui M, Gapihan G, Nguyen TT, et al. Targeting cancer stem cells to overcome chemoresistance. *Int J Mol Sci*. 2018;19:pii E4036.
26. Niewiadomski P, Kong JH, Ahrends R, Ma Y, Humke EW, Khan S, et al. Gli protein activity is controlled by multisite phosphorylation in vertebrate Hedgehog signaling. *Cell Rep*. 2014;6:168–81.
27. Hatayama M, Aruga J. Gli protein nuclear localization signal. *Vitam Horm*. 2012;88:73–89.
28. Harada T, Ohguchi H, Grondin Y, Kikuchi S, Sagawa M, Tai YT, et al. HDAC3 regulates DNMT1 expression in multiple myeloma: therapeutic implications. *Leukemia*. 2017;31:2670–7.
29. Amodio N, Stamato MA, Gulla AM, Morelli E, Romeo E, Raimondi L, et al. Therapeutic targeting of miR-29b/HDAC4 epigenetic loop in multiple myeloma. *Mol Cancer Ther*. 2016;15:1364–75.
30. Zaal EA, Berkers CR. The influence of metabolism on drug response in cancer. *Front Oncol*. 2018;8:500.
31. Liu H, Liu Z, Du J, He J, Lin P, Amini B, et al. Thymidine phosphorylase exerts complex effects on bone resorption and formation in myeloma. *Sci Transl Med*. 2016;8:353ra113.